On: 28 October 2013, At: 07:22
Publisher: Taylor & Francis
Informa Ltd Registered in England and Wales Registered Number: 1072954 Registered office: Mortimer House, 37-41 Mortimer Street, London W1T 3JH, UK

Computer Methods in Biomechanics and Biomedical Engineering

Publication details, including instructions for authors and subscription information:
http://www.tandfonline.com/loi/gcmb20

Validation of numerical flow simulations against in vitro phantom measurements in different type B aortic dissection scenarios

Eduardo Soudah[a], Paula Rudenick[b], Maurizio Bordone[a], Bart Bijnens[c], David García-Dorado[b], Arturo Evangelista[b] & Eugenio Oñate[a]

[a] Department of Biomedical Engineering, International Center for Numerical Methods in Engineering (CIMNE), Universitat Politècnica de Catalunya, Barcelona, Spain

[b] University Hospital and Research Institute Vall d'Hebron, Universitat Autònoma de Barcelona, Barcelona, Spain

[c] ICREA, PhySense - N-RAS, Universitat Pompeu Fabra, Barcelona, Spain

Published online: 25 Oct 2013.

To cite this article: Eduardo Soudah, Paula Rudenick, Maurizio Bordone, Bart Bijnens, David García-Dorado, Arturo Evangelista & Eugenio Oñate , Computer Methods in Biomechanics and Biomedical Engineering (2013): Validation of numerical flow simulations against in vitro phantom measurements in different type B aortic dissection scenarios, Computer Methods in Biomechanics and Biomedical Engineering, DOI: 10.1080/10255842.2013.847095

To link to this article: http://dx.doi.org/10.1080/10255842.2013.847095

Computer Methods in Biomechanics and Biomedical Engineering, 2013
http://dx.doi.org/10.1080/10255842.2013.847095

Taylor & Francis
Taylor & Francis Group

Validation of numerical flow simulations against *in vitro* phantom measurements in different type B aortic dissection scenarios

Eduardo Soudah[a]*, Paula Rudenick[b], Maurizio Bordone[a], Bart Bijnens[c], David García-Dorado[b], Arturo Evangelista[b] and Eugenio Oñate[a]

[a]*Department of Biomedical Engineering, International Center for Numerical Methods in Engineering (CIMNE), Universitat Politècnica de Catalunya, Barcelona, Spain;* [b]*University Hospital and Research Institute Vall d'Hebron, Universitat Autònoma de Barcelona, Barcelona, Spain;* [c]*ICREA, PhySense – N-RAS, Universitat Pompeu Fabra, Barcelona, Spain*

(*Received 22 April 2013; accepted 17 September 2013*)

An aortic dissection (AD) is a serious condition defined by the splitting of the arterial wall, thus generating a secondary lumen [the false lumen (FL)]. Its management, treatment and follow-up are clinical challenges due to the progressive aortic dilatation and potentially severe complications during follow-up. It is well known that the direction and rate of dilatation of the artery wall depend on haemodynamic parameters such as the local velocity profiles, intra-luminal pressures and resultant wall stresses. These factors act on the FL and true lumen, triggering remodelling and clinical worsening. In this study, we aimed to validate a computational fluid dynamic (CFD) tool for the haemodynamic characterisation of chronic (type B) ADs. We validated the numerical results, for several dissection geometries, with experimental data obtained from a previous *in vitro* study performed on idealised dissected physical models. We found a good correlation between CFD simulations and experimental measurements as long as the tear size was large enough so that the effect of the wall compliance was negligible.

Keywords: aortic dissection; computational fluid dynamics; *in vitro* phantoms; aortic diseases

1. Introduction

Aortic dissections (ADs) represent an important subgroup within the aortic diseases and are associated with a high morbidity and mortality (more than 50% in the acute phase) (Hagan et al. 2000). In particular, during the chronic phase, descending ADs (type B) result in a high long-term morbidity and mortality because of dissection recurrence, progressive lumen dilatation [particularly of the false lumen (FL)] and aortic rupture (Fattori et al. 2011).

The haemodynamics within the lumina is one of the underlying factors associated with the progression of chronic ADs (Gimbrone et al. 2000; Davies et al. 2005). The intra-luminal pressure has a direct effect on the aortic wall, determining local tissue mechanical stress. High pressures are therefore important risk factors for worse prognosis. Clinical observations show that the presence of large proximal tears (Evangelista et al. 2012) and a patent FL (Erbel et al. 1993) show a worse prognosis, which may be due to the high resultant FL pressures (Rudenick et al. 2013) and the associated wall stress. However, in clinical practice, intraluminal pressures cannot be measured non-invasively.

Currently, the use of numerical tools to simulate and characterise blood dynamics in the cardiovascular system is becoming more easily available. Especially, the application of computational fluid dynamic (CFD) simulations is emerging in the biomedical field and is presented as a reliable methodology to study cardiovascular diseases based on simulated haemodynamic parameters, such as pressures and wall shear stress. However, validation of these numerical results is of particular interest, and although there are some CFD studies oriented to the assessment of haemodynamics in type B ADs (Karmonik et al. 2011, 2012), in none of them a quantitative validation of the computational solutions has been performed.

Therefore, this study was aimed at applying a CFD methodology to the characterisation of haemodynamics in chronic ADs (through the assessment of pressures in the lumina) for four different (idealised) dissection geometries and validating it with the *in vitro* results from a previous study (Rudenick et al. 2013).

2. Methodology

The idealised geometric characteristics of the computational models, rheological data of the test fluid and the inflow and outflow boundary conditions for the numerical finite element method (FEM) simulations were based on the results from a previous *in vitro* study (Rudenick et al. 2013). We used the experimentally measured *in vitro* pressures, at different sites of the dissected segment, to validate the values predicted by the numerical model.

*Corresponding author. Email: esoudah@cimne.upc.edu

Figure 1. Reproduction of the FEM geometry.

2.1 Computational models

Based on the geometry and dimensions of the physical phantoms, used in the *in vitro* study (Rudenick et al. 2013), the computational three-dimensional (3D) finite element models and fluid meshes were constructed with GiD (CIMNE, Barcelona, Spain) (Figure 1) (CIMNE 2006; Bordone et al. 2010). The generic geometry consisted of two channels, the true lumen (TL) and the FL (surrounding the TL), connected by circular holes, representing the proximal and distal tears (Figure 2). The dimensions of the computational model were as follows: TL diameter, 14 mm; dissected segment diameter, 40 mm; FL length, 160 mm; dissection flap thickness, 2 mm and TL length, 390 mm. The centres of the proximal and distal tears were located at 175.5 and 320.5 mm, respectively, from the inlet of the model.

Four typical dissection geometries (Table 1), found in clinical practice, were numerically validated. These geometries represent different anatomic configurations, varying tear size (with a diameter of 4 mm = a 'clinically' small tear or 10 mm = a 'clinically' large tear), location (distal/proximal) and number (1/2).

The computational meshes consisted of ~1.5–2 million tetrahedral elements with a size range of 0.5–1.0 mm. A mesh sensitivity analysis was performed to ensure a smooth element with a tetrahedral element aspect ratio above 0.9 (ideal ratio = 1 for an equilateral triangle).

2.2 Numerical simulations

CFD simulations were performed using the CFD code Tdyn [CompassIS, Barcelona, Spain (Compass website)]. This code solves the Navier–Stokes equations for an incompressible and homogeneous Newtonian fluid using a stabilised FEM.

We used water at 25°C as perfusion fluid, with a density of 996 kg/m^3 and a viscosity of $0.86 \times e^{-3}$ kg/(m s).

Table 1. Scenarios validated in the study.

Case	Proximal tear (mm)	Distal tear (mm)
A	4	–
B	–	4
C	10	4
D	10	10

We assumed it to be incompressible, homogeneous and Newtonian, with no external forces applied on it.

The no-slip wall of the dissection model was assumed to be rigid (1a). Since in chronic dissections there is reduced flap motion, a rigid flap is a good first approximation. In addition, Leung et al. (2006) suggested that the difference in flow-induced pressure variations and consequent wall stress between rigid and elastic aortic models is negligible.

Time-dependent flow and pressure waveforms, obtained from the *in vitro* experiments, were applied at the inlet and outlet of the fluid domain, respectively. A fully developed parabolic velocity profile was applied at the inlet (1b), and a time-dependent normal traction, according to the luminal pressure profile, is imposed at the outlet (1c). Mathematically, these boundary conditions can be expressed as follows:

$$V = 0|_{\text{wall}}, \tag{1a}$$

$$u_z = 2(u(t))\left(1 - \left(\frac{2r}{d_r}\right)^2\right); \quad u_r = 0|_{z=0}, \tag{1b}$$

$$\tau_{nn} = \hat{n} \cdot p(t) I \cdot \hat{n}, \tag{1c}$$

where d_r is the inner radius of the TL, u_r is the Cartesian components of the velocity vector in the Z-direction and $u(t)$ and $p(t)$ are the time-dependent velocity and pressure waveforms taken from the *in vitro* experiments. Pressure boundary conditions are given by (1c), where τ_{nn} is the normal traction at the outlet, I is the standard identity matrix and $\hat{n}$ represents the normal vector of the respective boundary.

Due to the high Re number within the tear areas, a turbulence model is included. The turbulence model chosen was the Spalart–Allmaras model (Spalart 2000). The aim

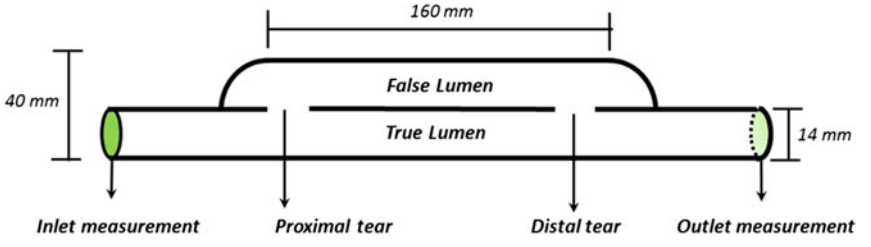

Figure 2. Generic geometry of a type B AD.

of this model is to improve the predictions obtained from algebraic mixing-length models to develop a local model for complex flows and to provide a simpler alternative to two-equation turbulence models. The model uses the distance to the nearest wall in its formulation and provides smooth laminar–turbulent transition capabilities. It does not require a grid resolution in wall-bounded flows as fine as the two-equation turbulence models, and it shows good convergence for simpler flows. The empirical results used in the development of the model were mixing layers, wakes and flat-plate boundary layer flows. The model gives very accurate predictions of complex turbulent flows. It also shows improvements in the prediction of flows with adverse pressure gradients compared to k–e and k–v models.

The CFD simulations were performed over a time period of 1.8 s (representing two cardiac cycles). The time integration method chosen was a backward Euler, using a biconjugate gradient non-symmetric solver (Barrett et al. 1994) in order to accelerate the calculation time performance. We used a pressure stabilisation of fourth order and automatic velocity advection stabilisation. The total CPU time for a single CFD analysis in a standard PC with Microsoft Windows XP, 32-bit, 4 GB RAM and dual-core 2.83 GHz CPU was about 10 h depending on the case.

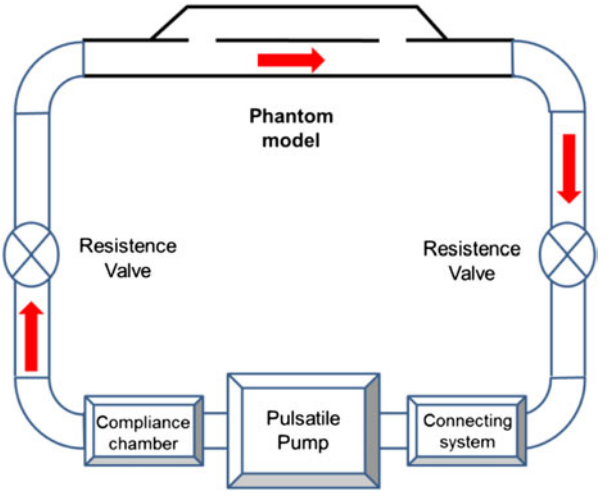

Figure 3. Schema of the dynamic flow circuit used for the *in vitro* experiments.

For each simulation analysis, we assessed the intra-luminal pressures in the FL and TL at the distal and proximal sites of the dissected model, where appropriate (Figure 2).

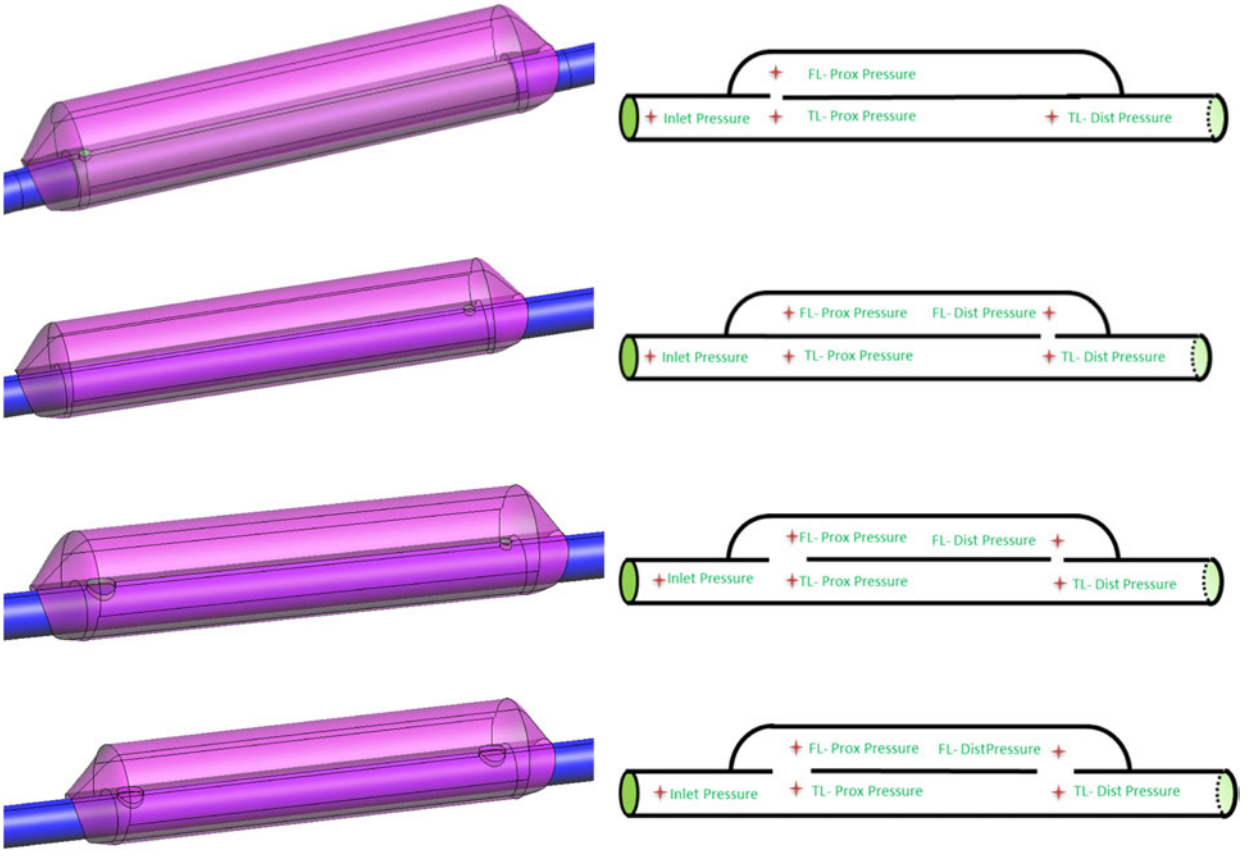

Figure 4. *In silico* FEM geometries (right) and schematic representation (left) for the four *in vitro* type B AD scenarios. From top to bottom: Case A, Case B, Case C and Case D.

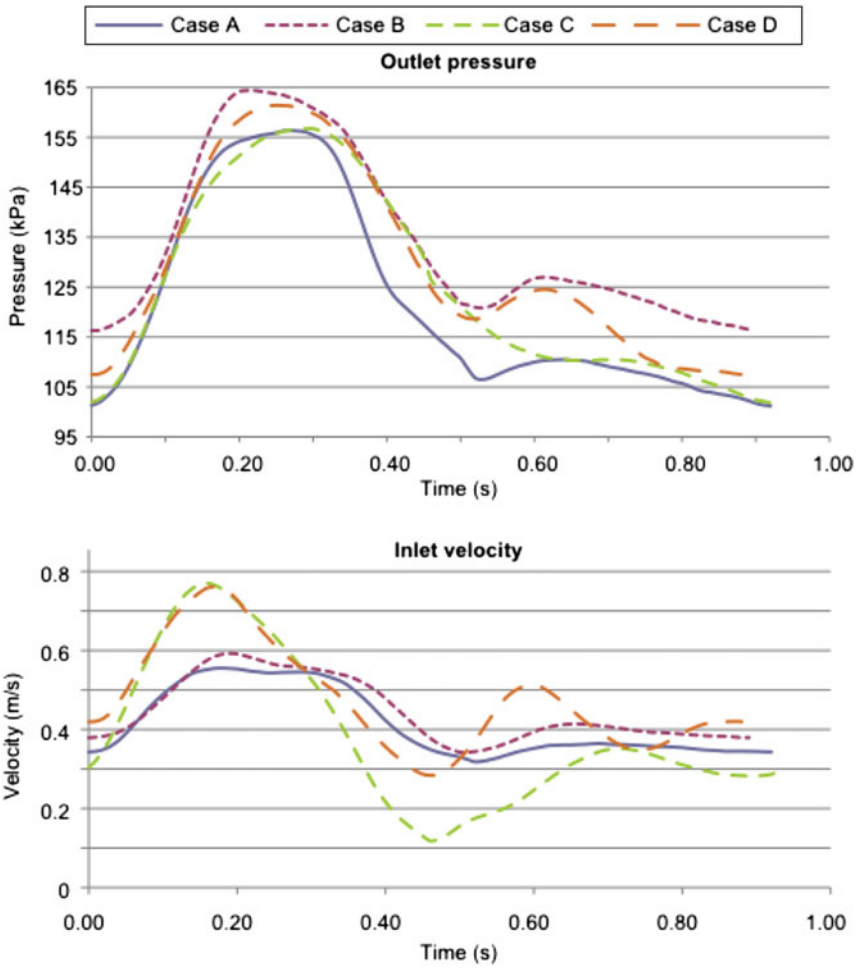

Figure 5. Pressure profiles measured at the outlet (top) and velocity profiles computed from the flows measured at the inlet (bottom) of the *in vitro* models for the four dissection scenarios.

2.3 *In vitro data*

For validation of the numerical simulations, we used the set-up and experimental data from a previous *in vitro* study (Rudenick et al. 2013).

The *in vitro* set-up consisted of a dynamic flow circuit mimicking the cardiovascular system, where a pulsatile pump, a compliance chamber, a dissection phantom and a collecting system were connected in series (Figure 3).

The phantom was a compliant model made of latex and silicone to recreate a simplified typical AD, where FL and TL are connected by circular holes resembling the tears in the dissection flap.

Pressures were measured, using retrograde catheterisation, within the FL and TL of the model at a proximal and distal site, using a pressure transducer (SPC-350 5F, Millar Instruments, Texas, USA). Only for Case A, the FL distal pressure could not be measured using this approach, since the catheter could not be bended 180°. Flow traces were measured at the inlet of the model, 15 cm before the dissected segment, with an ultrasonic flow meter (Transonic Systems, Inc., Ithaca, NY, USA). Pressure and flow measurements were registered/digitised using a PowerLab 16/30 with LabChat Pro acquisition and analysis software (ADInstruments, Colorado Springs, CO, USA). A more detailed description of the *in vitro* set-up can be found in Rudenick et al. (2013).

2.4 *In silico configurations and imposed boundary conditions*

Figure 4 shows the four configurations of ADs modelled together with the sites where *in vitro* pressures were available and *in silico* pressures were validated.

Figure 5 (top) shows the *in vitro* pressure profiles measured at the outlet in the hydraulic model for the four dissection configurations. Note that the pressure waveform was realistic, representing normal haemodynamic conditions in this area of the human aorta, with a peak pressure occurring at an interval 0.27–0.3 s and a biphasic diastolic period. Figure 5 (bottom) shows the velocity profiles

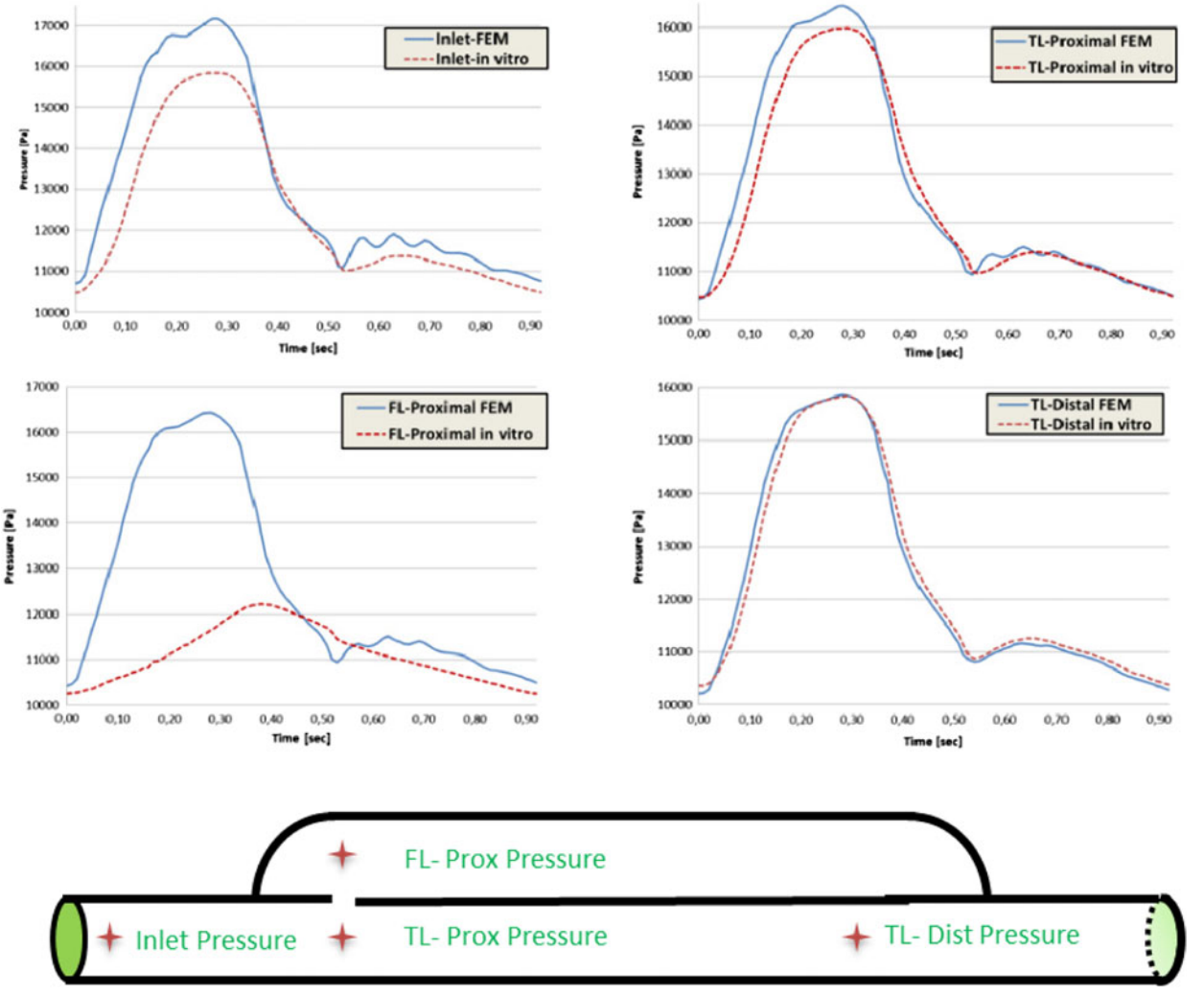

Figure 6. Case A: pressure comparison between *in vitro* (red dotted line) and FEM results (blue line) in proximal and distal TL sites.

computed from the flows measured at the inlet for the four configurations in the hydraulic model. The cycle period has a duration included between 0.88 and 0.95 s, with a peak flow occurring at 0.18–0.2 s.

3. Results

In this section, we compare the *in vitro* pressure waveforms with the numerical predictions. It is important to stress that none of the parameters involved in the simulation have been tuned, except for phase matching of the onset of the experimental and numerical systolic ejections during data post-processing.

3.1 Comparison between experimental and numerical results

Figures 6–9 show the comparison between the experimental and numerical pressure waveforms at four representative points for each of the dissected models. For each model, the inlet pressures together with relevant points in the TL and FL are presented. Table 2 provides the numerical values for the difference between measured and simulated cases.

In all cases, the inlet and TL pressures are very similar for the measured and simulated traces. Since the outlet pressure was used as a boundary condition, the further away from it towards the inlet, the more different the pressure curve, but differences are within acceptable levels. This can be caused by differences between the numerical and experimental models (rigid/elastic wall) and some uncertainties in the experimental set-up (e.g. the exact location and position of the catheter inside the aorta), which makes it more difficult to exactly compare the *in vitro* and *in silico* measurements.

For cases with at least one large hole (Cases C and D), the FL pressures are also very comparable between measurements and simulations.

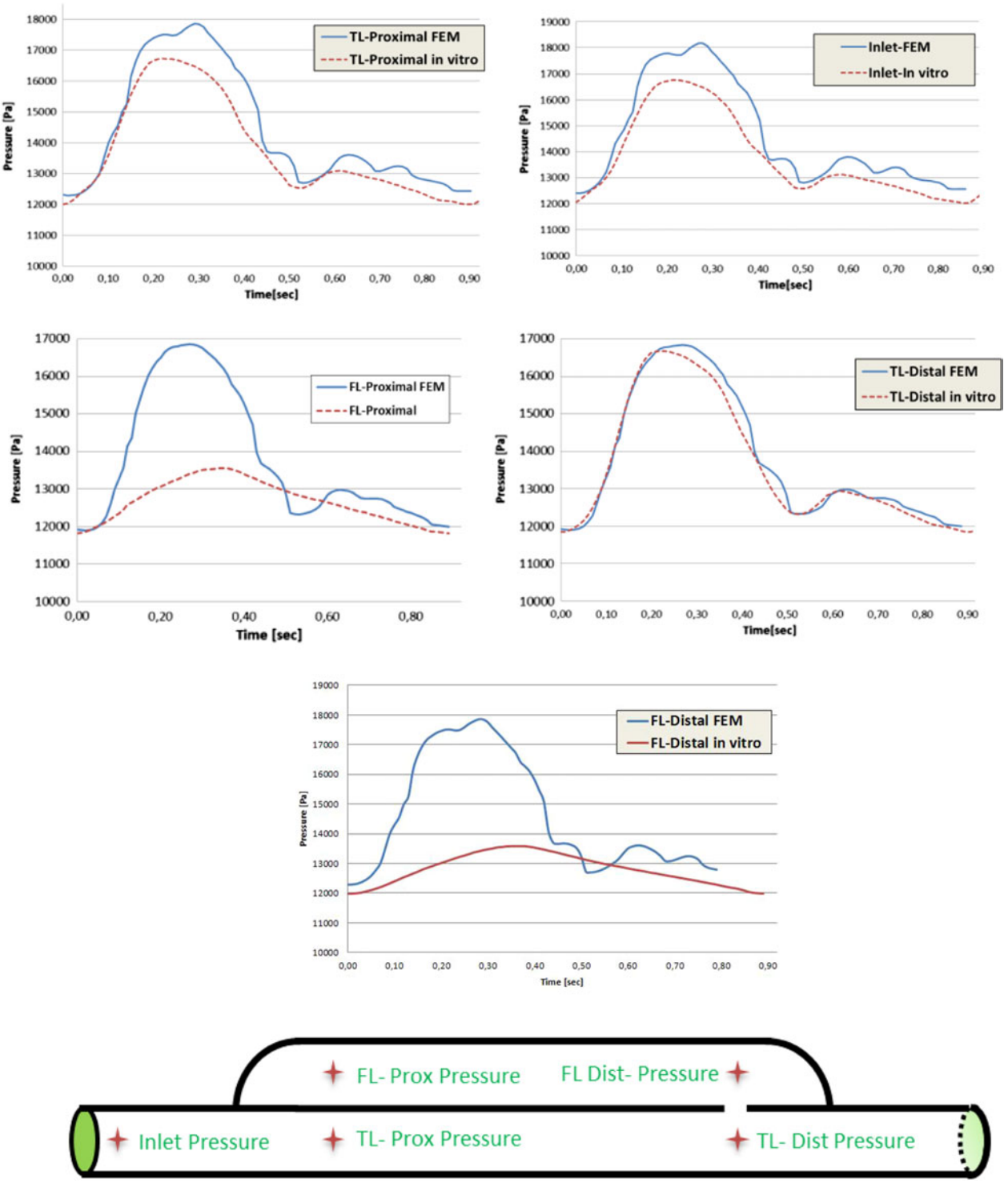

Figure 7. Case B: pressure comparison between *in vitro* (red dotted line) and FEM results (blue line) in proximal and distal TL sites.

Only for cases with only one small hole (Cases A and B), the FL measured pressures are clearly different from the simulated pressures, while the shapes and values of the profiles at the TL positions are quite similar. Since the measured values are much lower and seem to have been low-pass filters, the difference can be explained to a large extent by the difficulty to reproduce the experimental measurements in an elastic model with the numerical, rigid wall model.

In addition, all the pressure measurements were done using retrograde catheterisation (Evangelista et al. 2012),

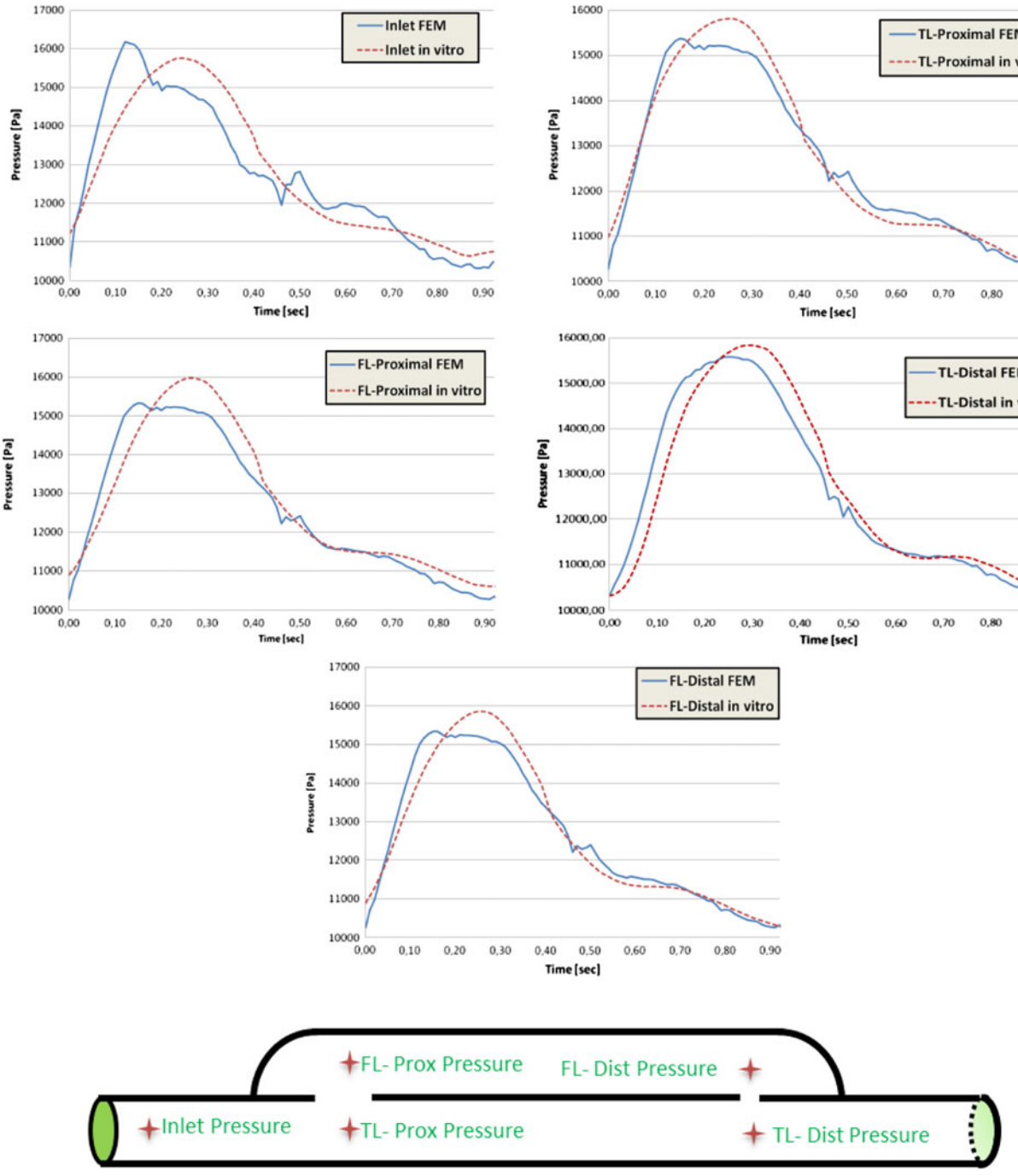

Figure 8. Case C: pressure comparison between *in vitro* (red dotted line) and FEM results (blue line) in the inlet, proximal and distal TL sites, and distal FL site.

which may have caused partial obstruction of the tears, thus reducing their effective size and altering the pressure measurements at the proximal and distal FL (especially for small holes as in Cases A and B).

Quantitatively, there are modest relative errors between the numerical and experimental waveforms (Table 2) for most of the measurements. Except for the FL with only small holes, these errors, depending of the point studied, are $<10\%$ for the pressure profile. In Case A, the TL error at the proximal section is $<9\%$ and at the distal section it is 0.3%, showing a good approximation for the TL in this configuration of AD. In Case B, pressure profiles at the TL are even closer to the experimental measurements and the mean error is around 2% at the

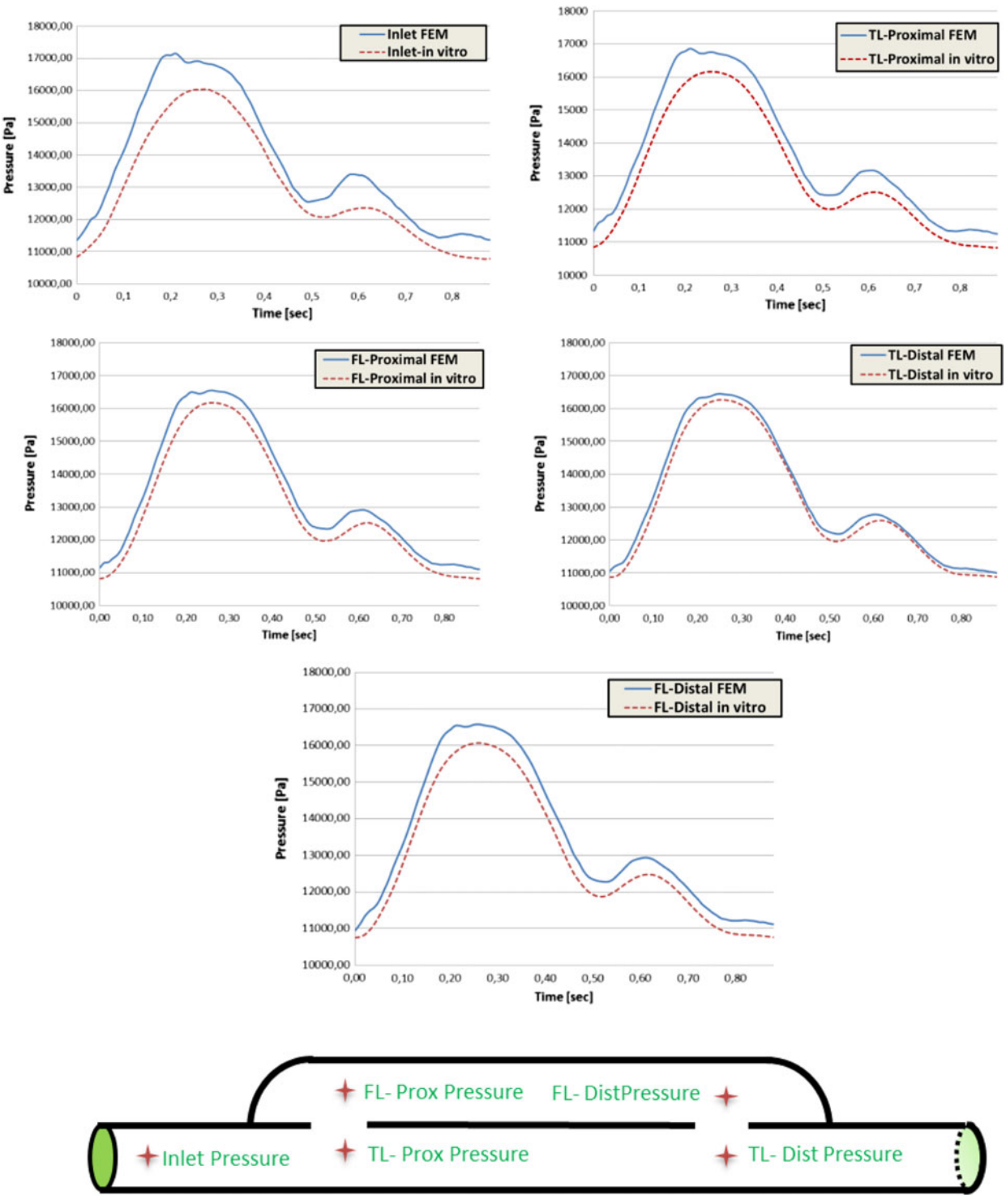

Figure 9. Case D: pressure comparison between *in vitro* (red dotted line) and FEM results (blue line) in the inlet, proximal and distal TL sites, and distal FL site.

proximal TL and 0.2% at the distal TL. In case C, in the inlet the error is 7.3%; in the distal FL and proximal TL points, the errors are around 5%; and in the proximal TL, the error is 4.64%. For the TL, the mean error in Case D is 3.64% with a maximum value of $<9.4\%$.

Therefore, we can conclude that the CFD simulation are able to capture the main features of pressure traces observed *in vitro*, such as the diastolic decay and peaking and steepening of pulse pressure for the different points measured in the TL and FL. Only in case of the presence of

Table 2. Error values in percentage for the different positions of measurements.

	Distal FL			Distal FL			Proximal FL			Proximal TL			Inlet		
Case	Min.	Max.	Average	Min.	Max.	Average	Min.	Max.	Average	Min.	Max.	Average	Min.	Max.	Average
A	–	–	–	−4.4	3.17	0.24	−4.62	2.24	−14.1	−8.96	4	−1.23	−26	9.4	−5.25
B	−28.1	8.55	−5.4	−6.07	4.58	0.2	−27.3	2.73	−8.37	−9.5	2.84	−2.05	−12.4	1.1	−4.71
C	−19.2	8.81	5.27	−8.47	5.1	2.6	−18.17	8.75	−0.85	16.47	9.01	4.64	25.2	13.63	7.3
D	−9.68	0.23	−3.64	−6.27	0.98	−1.81	−8.1	−2.2	−4.4	−23.8	−0.02	−10.15	−8.78	0.48	−3.4

only small tears, the FL pressures are not reliable using this approach.

4. Discussion

We have evaluated the use of a CFD methodology against *in vitro* measurements in four idealised configurations of chronic ADs. Following our previous findings (Rudenick et al. 2010), on the complementarity of *in vitro* and *in silico* approaches to assess haemodynamics in ADs of type B, this is the first attempt, to our knowledge, to quantitatively test the accuracy of a CFD model in the prediction of intra-luminal pressures in different clinical scenarios for this pathology.

Our results show the ability of the CFD model to capture the main features of the experimental pressure waveforms in the TL and also the FL, as long as the connection between TL and FL is through large holes. The average relative errors of the numerical predictions are $<10\%$ for the pressure profile at all locations studied. In general, relative errors are smaller at locations close to the outlet boundary condition, where the pressure matches its experimental counterpart. Discrepancies between experimental and numerical results may arise from a combination of the material properties of the *in vitro* and *in silico* models, from the way that *in vitro* pressures are measured and from the assumptions and simplifications of the CFD model. We are comparing a flexible physical phantom with a rigid computational model. Consequently, the elasticity of the latex wall of the FL has an important effect on damping the cyclic pressures and flows when entering the FL through a small connection, thus resulting in lower peak systolic pressures.

The pressures change along the geometry and it is difficult to determine the exact position of the transducer inside the phantoms and thus to exactly correlate the *in vitro* measurements with the *in silico* predictions.

Despite the detected differences, *in silico* and *in vitro* results show a similar behaviour, making them useful and complementary to study the properties of ADs (which in a lot of patients do have large communications). This encourages the use of our CFD methodology to characterise intra-luminal pressures in chronic ADs of type B.

While our approach is not an *in vivo* validation, it has the fundamental advantage of reducing the uncertainty of the parameters involved in the numerical simulation. While the phantom geometries are idealised models, their dimensions are based on clinical and experimental measurements, resulting in a generic model for parametric studies. Indeed, although the experimental set-up is only an approximation of a human AD of type B, it is able to reproduce pressure and velocity waveforms clearly representing those that can be expected physiologically (Evangelista et al. 2012).

AD is often associated with degeneration and diminished compliance of the aortic wall. Independent of the type of dissection (type A or B), most patients are elderly (Mehta et al. 2004; Tsai et al. 2006), with an aortic wall that has increased stiffness as a result of natural fatigue failure in response to permanent cyclic stresses. There are also other underlying factors in the clinical history of these patients that may lead to vascular remodelling and degradation of the aortic wall and thus reduce its elasticity, such as hypertension, genetics disorders as Marfan's syndrome or atherosclerosis. Under these considerations, a rigid-wall numerical model was supposed to be appropriate for modelling ADs. Nevertheless, it is not a good approximation when communication between the lumina is not large enough, in which the effects of wall compliance seem to play a key role in intra-luminal haemodynamics. The inclusion of wall compliance in the numerical simulations of these cases and a detailed analysis of how it affects intra-luminal haemodynamics are topics for further studies.

5. Conclusion

We have validated, in four different configurations of an idealised chronic AD, the ability of our CFD methodology to characterise intra-luminal pressures. The numerical simulations were able to capture the main pressure wave propagation observed in most phantom models, showing a good correlation with the experimental TL intra-luminal pressures as well with FL pressures in case of large communications. From a clinical point of view, intra-luminal pressure is one of the reported factors influencing AD in the long-term evolution. Intra-luminal pressure has a direct impact on the aortic wall, determining local tissue mechanical stress, and that is why one of the preferred treatments for patients with ADs of type B is an aggressive blood pressure control. However, it has been shown that the presence of large tears and patent FL is associated with long-term complications and mortality (Evangelista et al. 2012). However, currently, intra-luminal pressures are impossible to be measured in a non-invasive way and, therefore, it is still not well understood how they are affected by the communication between the lumina. Hence, the CFD methodology presented could provide an additional way for a better understanding of the haemodynamic conditions and related clinical evolution in patients with chronic ADs. Moreover, joining traditional measurements, from imaging analysis, together with CFD analysis, creating and using patient-specific or disease-specific geometries with accurate boundary conditions, might enable to obtain much more detailed information of haemodynamic behaviour of the aorta. The fusion of these approaches could offer improved information about wall stress conditions in aortic diseases, in particular in ADs, for predicting local remodelling induced by the same physiological conditions as in a patient studied.

Conflict of interest

There are no conflicts of interest between the authors of this paper and other external researchers or organisations that could have inappropriately influenced this work.

References

Barrett R, Berry M, Chan TF, Demmel J, Donato JM, Dongarra J, Eijkhout V, Pozo R, Romine C, Van der Vorst H. 1994. Templates for the solution of linear systems: building blocks for iterative methods. 2nd ed. Philadelphia (PA): SIAM.

Bordone M, Oñate E, Rudenick PA, Bijnens BH, Soudah E. 2010. Study of flow phenomena in aortic dissection. Barcelona: GiD Congress.

CIMNE. 2006. GiD – The personal pre and postprocessor. Available from: http://www.gidhome.com/

Compass website. TDYN. Available from: http://www.compassis.com

Davies PF, Spaan JA, Krams R. 2005. Shear stress biology of the endothelium. Ann Biomed Eng. 33:1714–1718.

Erbel R, Oelert H, Meyer J, Puth M, Mohr-Katoly S, Hausmann D, Daniel W, Maffei S, Caruso A, Covino FE, et al., 1993. Effect of medical and surgical therapy on aortic dissection evaluated by transesophageal echocardiography. Implications for prognosis and therapy. The European Cooperative Study Group on Echocardiography. Circulation. 87 (5):1604–1615.

Evangelista A, Salas A, Ribera A, Ferreira-González I, Cuellar H, Pineda V, González-Alujas T, Bijnens B, Permanyer-Miralda G, García-Dorado D. 2012. Long-term outcome of aortic dissection with patent false lumen: predictive role of entry tear size and location. Circulation. 125(25):3133–3141.

Fattori R, Mineo G, Di Eusanio M. 2011. Acute type B aortic dissection: current management strategies. Curr Opin Cardiol. 26(6):488–493.

Gimbrone MA, Jr, Topper JN, Nagel T, Anderson KR, Garcia-Cardeña G. 2000. Endothelial dysfunction, hemodynamic forces, and atherogenesis. Ann N Y Acad Sci. 902:230–240.

Hagan PG, Nienaber CA, Isselbacher EM, Bruckman D, Karavite DJ, Russman PL, Evangelista A, Fattori R, Suzuki T, Oh JK, et al., 2000. The International Registry of Acute Aortic Dissection (IRAD): new insights into an old disease. JAMA. 283(7):897–903.

Karmonik C, Bismuth J, Davies MG, Shah DJ, Younes HK, Lumsden AB. 2011. A computational fluid dynamics study pre- and post-stent graft placement in an acute type B aortic dissection. Vasc Endovasc Surg. 45(2):157–164.

Karmonik C, Partovi S, Müller-Eschner M, Bismuth J, Davies MG, Shah DJ, Loebe M, Böckler D, Lumsden AB, von Tengg-Kobligk H. 2012. Longitudinal computational fluid dynamics study of aneurysmal dilatation in a chronic DeBakey type III aortic dissection. J Vasc Surg. 56 (1):260–263.

Leung JH, Wright AR, Cheshire N, Crane J, Thom SA, Hughes AD, Xu Y. 2006. Fluid structure interaction of patient specific abdominal aortic aneurysms: a comparison with solid stress models. Biomed Eng Online. 5:33.

Mehta RH, Bossone E, Evangelista A, O'Gara PT, Smith DE, Cooper JV, Oh JK, Januzzi JL, Hutchison S, Gilon D, et al.,

2004. Acute type B aortic dissection in elderly patients: clinical features, outcomes, and simple risk stratification rule. Ann Thorac Surg. 77(5):1622–1628.

Rudenick PA, Bijnens BH, García-Dorado D, Evangelista A. 2013. An *in vitro* phantom study on the influence of tear size and configuration on the haemodynamics of the lumina in chronic type B aortic dissections. J Vasc Surg. 57 (2):464–474.

Rudenick PA, Bordone M, Bijnens BH, Soudah E, Oñate E, García-Dorado D, Evangelista A. 2010. A multi-method approach towards understanding the pathophysiology of aortic dissections – the complementary role of *in silico*, *in vitro* and *in vivo* information. Paper presented at: Engineering in Medicine and Biology Society (EMBC), 2010 Annual International Conference of the IEEE. Digital Library. p. 2509–2512.

Spalart PR. 2000. Strategies for turbulence modelling and simulations. Int J Heat Fluid Flow. 21(3):252–263.

Tsai TT, Evangelista A, Nienaber CA, Trimarchi S, Sechtem U, Fattori R, Myrmel T, Pape L, Cooper JV, Smith DE, et al., 2006. Long-term survival in patients presenting with type A acute aortic dissection: insights from the International Registry of Acute Aortic Dissection (IRAD). Circulation. 114(1 Suppl.):I350–I356.